8th semester Open lab
Report

Magnetostriction with LabVIEW

Submitted by

Gaurav Kanu
1811067
4th year Integrated MSc
National Institute of Science Education and Research

Under the supervision of

Dr. Ritwik Das
Dr. Gunda Santosh Babu
National Institute of Science Education and Research

School of Physical Sciences

This report is submitted for the partial fulfillment of the course P-443/444

Study of Magnetostriction with Labview

Gaurav Kanu

National Institute of Science Education and Research, Jatni, Khurda, Bhubaneshwar, Odisha 752050
e-mail: gaurav.kanu@niser.ac.in
Roll.no: 1811067

Submitted on: February, 27, 2022 ; Presentation on: February, 21, 2022

ABSTRACT

Ferromagnetic materials have naturally occurring property of magnetostriction such that, under the application of external magnetic field it changes it's dimensions. The change in the dimensions of materials take place upto the order of 10^{-6} and to measure the change Michelson's interferometer is used. In this report a detailed study of theory behind the magnetostiction pheonomena, simulation for measurement using Michelson's interferometer and proposal for scope of improvements and answering the question raised during the lab presentation is done.

1. Objective

1. To study Michelson's interferometer.
2. To do a detailed study of magnetostriction property and how it changes in materials iron, nickel and copper.

2. Apparatus

- Base plate with rubber feet
- HeNe Laser
- Adjusting supports(3)
- Surface mirrors(4)
- Magnetic base(7)
- Beam splitter, 50:50
- Plate holder
- Lens with mount, f = +20 mm
- Lens holder for base plate
- Screen
- Coil, N = 1200, 4 , Faraday Modulator
- Metal rods for magnetostriction (Fe,Ni,Cu)
- Power supply
- Digital multimeter
- Battery, 9 V(2)
- Connecting cord, l = 500 mm
- Photodiode Amplifier(AD711 opamp)
- Oscilloscope
- Computer with LabVIEW software installed

3. Introduction

Magnetostriction is a fundamental property of any material with unpaired spin available. The production of mechanical force as a result of magnetic effect is even seen in our everyday life. Magnetostriction has general applications like medical devices and industrial vibrators, ultrasonic cleaning devices, underwater sonar, vibration or noise control systems. It is therefore motivating to analyse this effect in detail in an experiment and propose theory of microscopic interactions that lead to this on a macroscopic scale. Magnetostrictive effect in a crystal is generally of three types:

- Bulk stress where the material changes its physical dimensions, (Inverse Villari effect)
- Shear stress where the material faces a rotational force due to the field, and (Inverse Matteuci effect)
- Torsional stress where the material faces a "twisting" effect on the magnetic field. (Inverse Wiedemann effect)

We measure the strain in our material arising due to bulk stress in this experiment. Usually, the volume change of such magnetostrictive materials is of the order 10-6. Hence, in order to measure this effect, we take a solid rod of our samples where the dimension of its length is the most prominent one. In this way, assuming the radius changes negligibly, we can deduce the change in length which is now m. To measure the changes in this scale, we need to use a Michelson interferometer operating at wavelength of 600-700nm such that the change in length is well perceived by any changes in length of the order of this wavelength.

4. Theory of Magnetostriction

4.1. *Crystal anisotropy*

Crystal anisotropy is the property of our lattice to prefer change in free energy in one preferred direction over others. This arises due to the inherent symmetry of the way our atoms are arranged in the sample lattice. In ferromagnetic materials where domain formation exist, energy is decreased by rearrangement of these domains and thus, our domains prefer to align along an axis. This is called the "easy axis" of the crystal. A crystal structure can have multiple easy axes. Similarly, in the similar sense there is also herd axis where the crystal feels the least change in energy if realigns its domains. This is called the "hard axis". This anisotropy energy has components of its tensors described by the symmetries present in the crystal. Based on that, it will only have certain independent components existing that is a material specific quantity.

The general anisotropy energy density of a cubic crystal is given by:

$$e_{K_e} = K_{\mathrm{c1}}\left(m_1^2 m_2^2 + m_2^2 m_3^2 + m_3^2 m_1^2\right) + K_{\mathrm{c2}}\left(m_1^2 + m_2^2 + m_3^2\right) \qquad (1)$$

where m_i is the magnetisation of our ferromagnetic domain along the cubic axes, K_{c1}, K_{c2} are the independent parameters determined by the material properties. Using this effect the energy surfaces of a cubic crystals can be shown and the easy axis can be seen to be affected by the parameters.

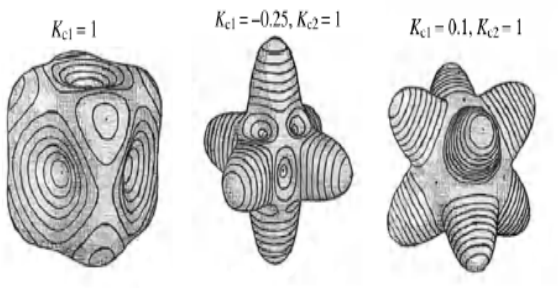

Fig.1: Energy surfaces of a cubic lattice for different parameters. The spikes correspond to higher energies than the valleys. The corresponding easy and hard axes respectively are: (a) <001>, <111>. (b) <011>, <001>. (c) <001>, <111>.

For iron and nickel samples the crystal structure is FCC. Correspondingly in our given samples the easy and hard axes play a strong role indetermining the extent of domain alignment along the applied stress direction. Although the saturation domain alignment is independent of the direction of the stress, the effect of anisotropy is significantly different in regimes where all spins have not aligned along the stress direction.

Figure below shows the easy axes of typical FCC, BCC and hexagonal lattices.

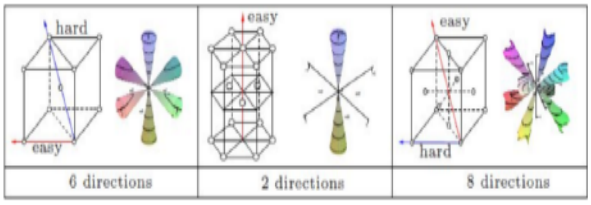

Fig.2: Easy and hard axes of BCC (a), Hexagonal (b), and FCC (c) crystals.

4.2. ***Magnetostriction and strain***

Magnetostriction arises in the microscopic scale chue to the existence of spin-orbital interactions and an anisotropy within our crystal. Spin orbit coupling is the phenomenon where the relativistic corrections of an electron moving around with an angular momentum couples its own spin with the angular spin resulting in finer energy splits during the application of an external field H. This effect is highly influenced by the interatomic distance (that decides the extent of overlap between atomic orbitals) and the exchange energy (the energy that looks at the neighbouring atoms and tries to align its spin along the neighbour's). As a result of these, we have a potential landscape that is dependent on both the applied field H, and the interatomic distance. Therefore, our lattice now tries to attain a stable equilibrium by rearranging its domains as a consequence of H. The decrease in the energy density along the easy axis leads to a stress force generated which causes elastic deformations. Spontaneous magnetostrictive elongation of a cubic crystal is given in A. Hubert by equating the components of magneto anisotropy energy of a cubic crystal with its stress tensor components as:

$$\frac{\delta l}{l} = \frac{3}{2}\lambda_{100}\left(\sum_{i=1}^{3} a_i^2 m_i^2 - \frac{1}{3}\right) + 3\lambda_{111}\sum_{i>k} m_i m_k a_i a_k \tag{2}$$

where a_i is the elongation of the crystal along the direction a, λ_{ijk} are the parameters of our stress tensor in cubic crystal dependent in the elastic

properties of our material, m_i is the component of magnetisation along a_i. The magneto-elastic stress tensor of our sample due to the existence of magnetisation in is given by:

$$\sigma_{ii} = -3C_2\lambda_{100}\left({m_i}^2 - \frac{1}{3}\right) \tag{3}$$

$$\sigma_{ik} = -3C_3\lambda_{111}\,(m_i m_k) \tag{4}$$

C_1, C_2 are constants in our elastic tensor coefficients in a cubic crystal. We notice bulk stress generated σ_{ii} is dependent on just the m_i and some material dependent constants. On ignoring the details of shear stress and considering all practical lattice defects and extent of magnetisation **m** due to **H**, we can write from (2) the overall effect of H to produce $s = \frac{\delta l}{l}$ as:

$$s = -\gamma(H)\mu(H)\frac{H}{E} \tag{5}$$

where E is the elasticity module corresponding to the direction of H

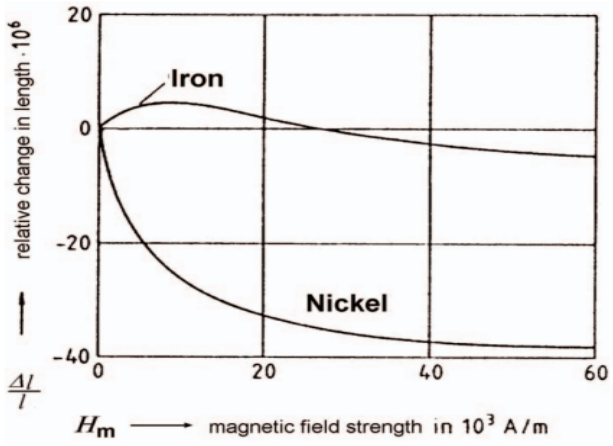

Fig.3: Literature values of Magnetostriction of Iron and Nickel. Here in Strain vs Magnetic field, Iron shows positive magnetostriction at low H and negative at high H while nickel shows negative magnetostriction throughout.

In the low H regime, where we haven't achieved saturation of domain alignment along H, we have a linear relation of strain vs ext.field. However, the strain reaches a saturation on high H operations as we cant have infinite stretching of our material and non-magnetic interactions appear in our crystal energy at those situations.

The inverse effect of our experiment is the *"Villari Effect"* where the applied stress generates spontaneous alignment of domains and result in magnetisation. Figure below shows this on application of stress in y-axis resulting in a domain arrangement along x-axis.

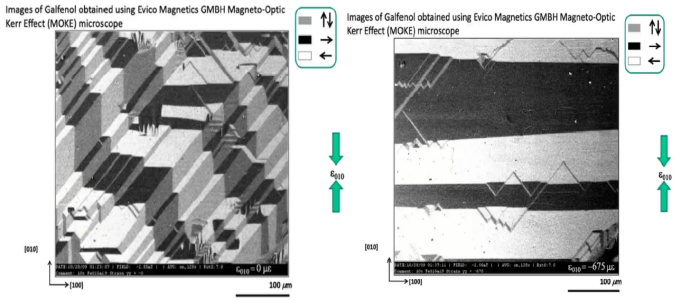

Fig.4: Rearrangement of domains in a strongly magnetostrictive Galfenol material seen under a MOKE image.

5. Theory of Michelson interferometer and simulations

5.1. *Theory of the interferometer*

Michelson interferometer is a setup where we take the help of two mirrors and a beam splitter to generate two coherent light sources spaced apart along the axis where the light beam travels. This interferometer is capable to distinguish length changes that occur in the order of the wavelength λ used. The setup is shown in Figure 5.

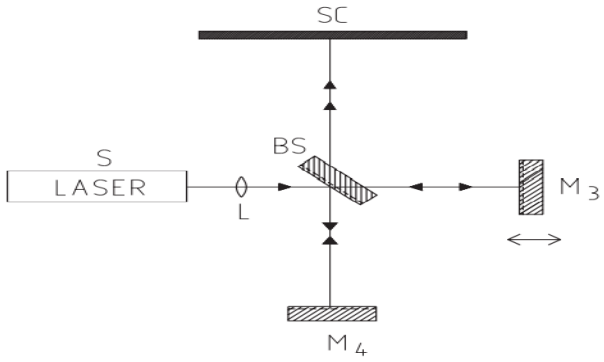

Fig.5: A schematic of Michelsons interferometer used.

When a coherent laser light hits a lens L, it is converted into a spherical wave and this proceeds to get divided into two light rays at BS. One reflects and reaches M4, and the other transmits and reaches M3. M4 is fixed while M3 is movable. These two rays, after reflecting back from the mirrors hit the beam splitter again and now the transmitted M4 ray interferes with reflected M3 to produce interference patterns at screen. During this process, M3 and M4 produce two virtual images that act as two coherent light sources. Coherent because both the light rays are in same phase at all times as they are generated by the same laser source S. We realise this by rotating M4 90^o clockwise parallel to M4 and removing the BS by considering each of these mirrors independently produce images of S as shown in Figure 6.

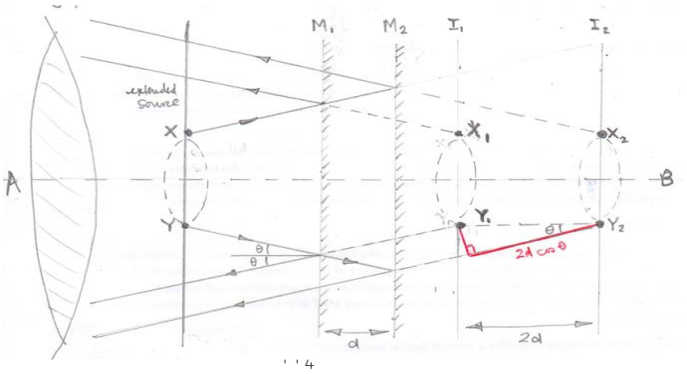

Fig.6: Equivalent ray diagram of our Michelson interferometer. d is the distance between the both mirrors while they form light sources with 2d distance between them.

In the above Fig.6 we see that different radial distances from the center of the screen have different phase differences from the two sources. If the light source X_1Y_1 travel x distance to reach a point in screen, the light source X_2Y_2 has to travel an additional distance of $2d$ Cos (θ). The E-field wave propagating in air is given by:

$$E = E_0 e^{i(kx-\omega t)} \tag{6}$$

Where k is the wave vector defined by $k = \frac{2\pi}{\lambda}$ and ω is the frequency of light propagating. If (6) is used to generate two E-waves with a path difference of δx, we have:

$$E = E_0 \,\mathrm{Sin}(kx - \omega t) + E_0 \,\mathrm{Sin}(k(x + \delta x) - \omega t) \tag{7}$$

Intensity of the light at a point is defined by:

$$I = \tfrac{1}{2}\epsilon_0 E^2 = \tfrac{1}{2}\epsilon_0 E_0^2 (\mathrm{Sin}(kx - \omega t) + \mathrm{Sin}(k(x + \delta x) - \omega t))^2 = \tfrac{1}{2}\epsilon_0 E_0^2 \left(2\,\mathrm{Sin}\left(\tfrac{(2kx+\delta x-2\omega t)}{2}\right)\mathrm{Cos}\left(\tfrac{k(\delta x)}{2}\right)\right)^2 \propto \mathrm{Cos}^2\left(\tfrac{k\delta x}{2}\right) \tag{8}$$

Hence, at constructive interferences, we have the argument inside cosine term an integral multiple of π

$$\frac{k\delta x}{2} = \frac{2\pi\delta x}{2\lambda} = n\pi \tag{9}$$

$$\delta x = 2d\,\mathrm{Cos}(\theta) = n\lambda \tag{10}$$

This is the interference we wish to read at the center of our screen as the mirrors move.

5.2. *Simulation of interferometer*

We have performed a Mathematica simulation of the fringes produced in the screen by using (9) and substituting (10) obtained from Fig. 6. (11) is the key formula used to produce the simulation results. The codes of simulation are given in Appendix.

$$\mathrm{Cos}(\theta) = \sqrt{1 - \frac{r^2}{f^2}} \tag{11}$$

$$I = 1 + \mathrm{Cos}\left[\frac{2\pi}{\lambda} 2d \sqrt{1 - \frac{r^2}{f^2}}\right] \tag{12}$$

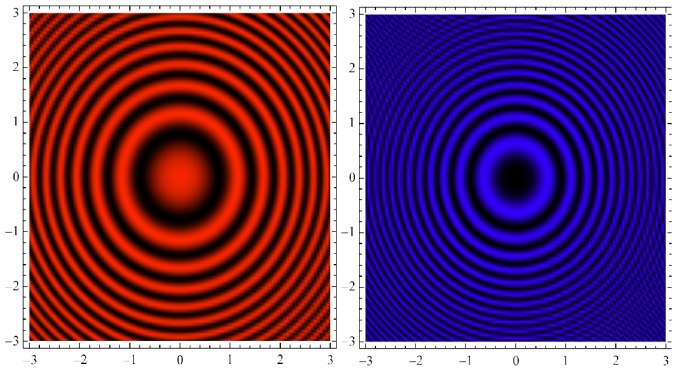

Fig.7: Haidinger fringes obtained at the screen with mirrors at 96.5μm and focus of lens f=20 mm. (a) λ=700 nm. (b) λ=400 nm

Figure 8 shows the central fringe decreases its radius and the fringes come closer together as the mirror moves farther away.

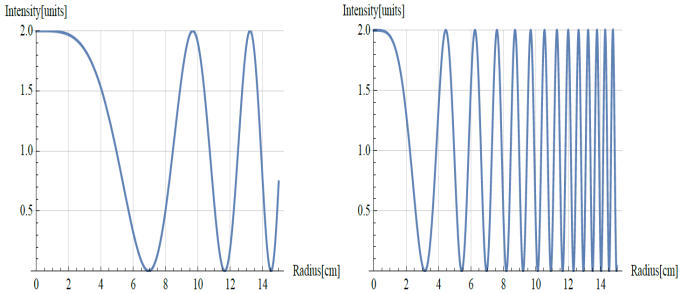

Fig.8: Fringes intensity with radius at mirror distance: (a) d=1.6 μm. (b) d=7 μm

Figure 9 shows the intensity peals obtained at the center of the screen as the mirror changes its distance for the laser light source being used.

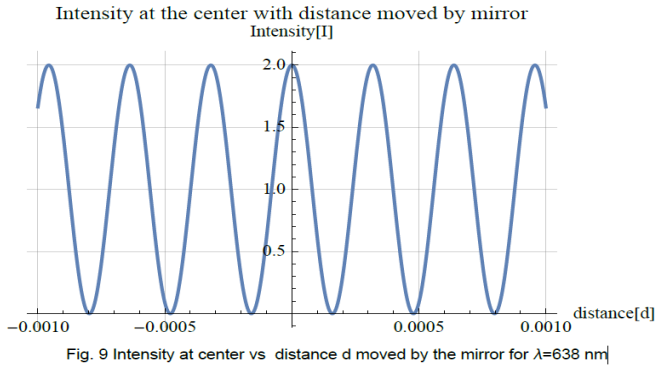

Fig.9: Intensity at center vs distance d moved by the mirror for λ=638 nm

6. Experimental setup

The magnetostriction experiment setup consisits of Michelson interferometer, a long solenoid acting as the magnetic field source and samples - Copper (Cu), Nickel (Ni), Iron (Fe) to study magnetostriction, detector and power source.

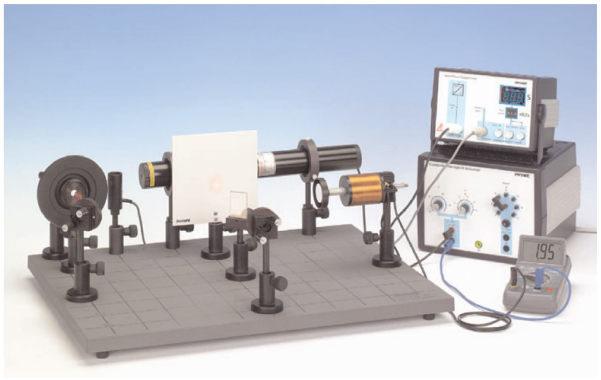

Fig.10: Experimental setup.

The schematic of the experimental setup is shown in figure 11. The light beam leaves the He-Ne laser and gets reflected through the first mirror M_1 and after that it passes through a focusing lens to get circular wave-front, the light beam again reflects through mirror M_2 and then it gets splitted by a 50/50 beam splitter (BS), the 50% of the beam gets reflected towards the mirror M_4 and remaining 50% of the beam gets transmitted through the BS via refraction and this transmitted beam gets refracted towards mirror M_3. The light beams at M_3 & M_4 reflects back towards the BS and this time both the light beams interfere and form circular fringes at the screen. Here M_4 is the immovable mirror and M_3 mirror moves by magnetostriction happening in the sample loaded via which the changes in the fringes is measured and thus change in dimension of the sample.

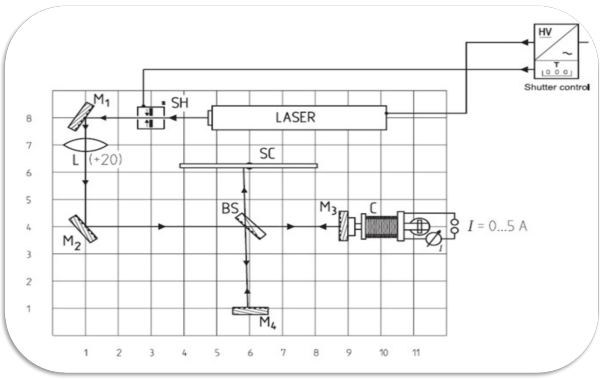

Fig.11: Schematic of experimental setup.

Connecting the coil to the power supply (connect the multimeter in series between the coil and the power supply to measure the current)and setting the DC voltage to maximum, the current is slowly readjusted and the changes from maximum to maximum (or minimum to minimum) in the interference pattern is recorded.Same procedure is done for different samples. For setting up photodiode, a photodiode amplifier circuit is first made using opamp AD711. Its amplification and gain are checked by connecting to an oscilloscope. For measuring the DC voltage for DC current change, beam expander is removed and the interference point is made to fall on the photodiode. Changing the current manually,we record the voltage change. High voltage corresponds to a maxima and low voltage corresponds to a minima. So the number of fringes shrinking or sourcing is noted.

6.1. *He-Ne Laser*

The acronym LASER stands for "Light Amplification through Stimulated Emission of Radiation". The light emitted by a

laser has very special properties which distinguish it from the light given off by an ordinary source of electromagnetic radiation, such as a light-bulb. These special properties make it possible to use laser's for very unusual purposes for which ordinary, even nearly-monochromatic light is not suitable.

6.1.1. **Properties of the laser light:**

- The light is extremely monochromatic with wavelength λ = 632.8 nm.
- The laser has a high "temporal coherence". The distance over which the waveform remains similar to a sine-wave is called the coherence- length of the beam, Lc, and it is typically about 10-30 cm for commercial He-Ne lasers.
- The laser light is unidirectional and aligned parallel to the body of laser.
- The light is "spatially coherent". The phase of radiation is nearly constant throughout the cross-sectional width of the beam.
- A Brewster-window is often inserted in the laser by the manufacturer to produce light with a definite state of linear polarization.

6.1.2. **Mechanism of laser:**

A He-Ne laser consists of a hollow tube filled with 90 percent He and 10 percent Ne gases and fitted with inward- facing mirrors at the ends of the cavity. The combined pressure of the two gases is approximately 1 Torr (1/760 atmospheres).

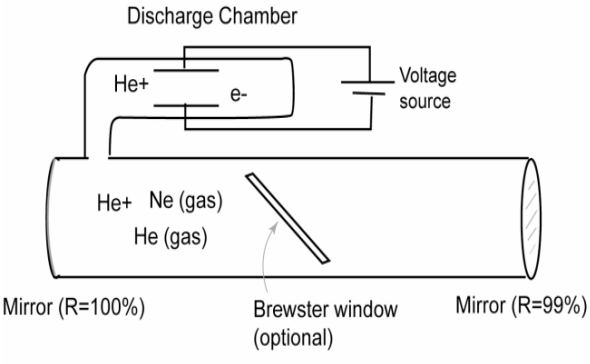

Fig.12: Schematic of Laser cavity.

An He-Ne laser works by exciting Neon atoms in the gas. The 632.8 nm optical light emitted by the laser is generated in the process when the Neon atoms decay from an excited state to an ordinary state.

6.1.3. **Quantum theory of laser:**

In quantum theory, a molecule can only exist in a discrete set of states $Z_1, Z_2, ...Z_n$ with energies $e_1, e_2, ...e_n$. A molecule can be promoted from state (call it "Z_n") to a higher energy state ("Z_m") by absorbing a photon with frequency, ν, proportional to the energy separation between these two states.

$$h\nu = e_m - e_n \quad (e_m > e_n) \tag{13}$$

The molecule can decay from a state Z_m to a lower energy state Z_n, by emitting a photon of that same frequency. This is slightly more complicated because there are two ways this can happen:

1. The molecule collides with a photon of frequency $h\nu = e_m - e_n$ and emits a second photon. The two photons leaving the molecule have identical frequency, phase, polarization, and travel in the same direction. This is called "stimulated emission". It is the reason why lasers generate light with the unusual properties mentioned above.
2. The molecule can decay on its own, emitting a photon of frequency $h\nu = e_m - e_n$, seemingly without any prompt from the external world. This is called "spontaneous emission." This photon will travel in a random direction with a random phase.

It is important to mention transition between any pair of states can be forbidden or suppressed (made to happen infrequently) by selection rules.

Helium and Neon are noble gases containing only one atom per molecule. Consequently, the states of a Helium and Neon molecule are relatively simple: The different states of an Ne molecule correspond to the different orbitals that electrons that surround the Ne atom can occupy. Radiation striking the Neon atoms causes the electrons circling these atoms to jump from one orbital to another.

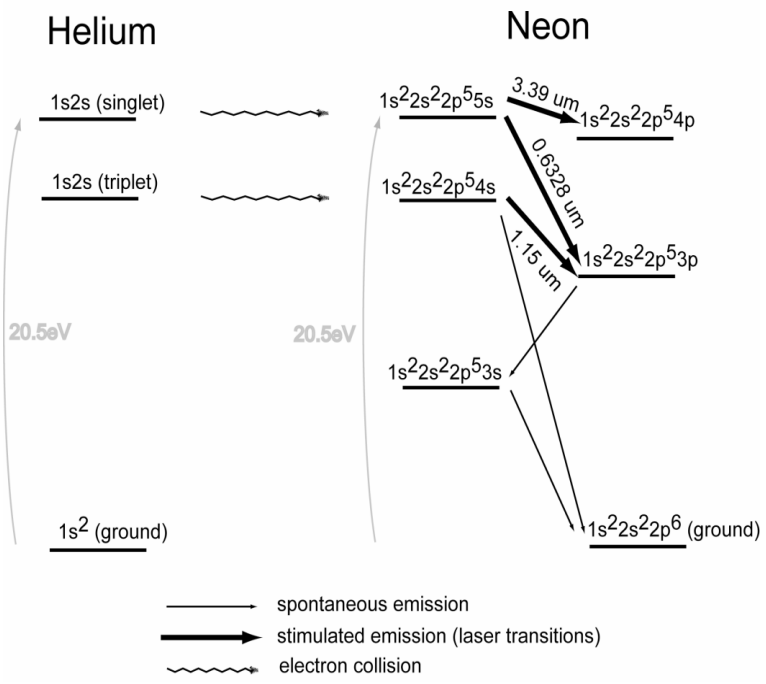

Fig.13: Excited states of the He and Ne atoms.

An electrical discharge created by strong electric fields ionizes the He gas. Helium in its lowest energy state has an electron configuration of $1s^2$. After the ionized He+ atoms recombine with their electrons some of the Helium atoms end up in the 1s2s-singlet state. Once in this state, the He atoms are forbidden from spontaneously making radiative transitions to lower energy states by quantum selection rules.

However, excited He atoms can decay through collisions with other atoms. The purpose of He atoms is to act as a power source for the Ne atoms, kicking them up into an excited state. If an excited He atom collides with an Ne atom, there is a finite probability that during the time over which the two atoms are in close proximity with each other, the excited He atom can transfer its energy to the Ne atom. This requires that there is a vacant

excited state for the Ne atom to jump to. Fortunately, Neon has an excited state whose excitation energy nearly matches the excitation energy of the He atom (20.5 eV, Figure 13).

Furthermore the excited Ne atom is allowed to decay by spontaneous emission to a lower energy state, releasing a photon of energy. That lower energy state, in turn may decay to a lower energy state, until the ground state of Ne is reached. Of course, at each transition, a photon is generated, and there are many such transitions, but we can only see the ones which generate light in the visible spectrum. The transition that generates 632.8 nm photons occurs when the outermost Ne electron decays from the 5s to the 3p orbital (Figure 13) .

This starts a chain reaction. As a 632.8 nm photon leaves one Ne atom, it collides with another excited Ne atom stimulating the emission of a second photon with identical direction, frequency, and phase. The light flux has been amplified by a factor of two! These two identical photons collide with other Ne atoms and increase the amplification. Photons emitted parallel to the long axis of the laser strike the mirrors and are reflected back along the axis, further increasing the amplification. (By contrast, photons which don't point down the axis of the cylinder will quickly leave the cavity and have fewer chances to collide with Ne atoms. These photons will not be amplified.) One of the mirrors is about 1% transmissive and this 1% of the laser light is the output of the laser.

6.2. ***Beam splitter 50:50***

A beam splitter is an optical device that splits beams (such as laser beams) into two (or more) beams. Beam splitters typically come in the form of a reflective device that can split beams into exactly 50/50, half of the beam being transmitted through the splitter and half being reflected.

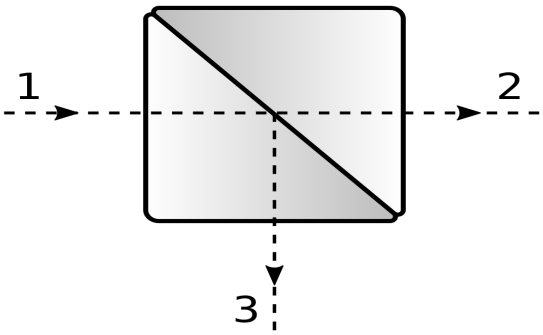

Fig.14: 50/50 beam splitter.

Type of beam splitters:

1. Cube beam splitters are made from two triangular glass prisms glued together (Fig.15). The thickness of the glue is carefully adjusted so that, for certain wavelengths of light, half the light that enters the cube is reflected 90^o and the other half is transmitted through the cube in the same direction as it entered (Figure 15).
2. Plate beam splitters are half-silvered mirrors are a sheet of glass or plastic with a very thin coating of reflective metal, usually aluminum. The thickness of the metal coating allows for half the light to be transmitted, and the other half to be reflected at 90^o (Figure 16).

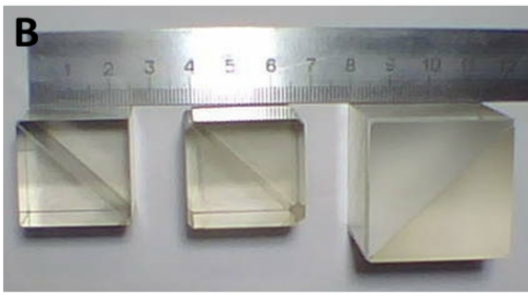

Fig.15: Cube beam splitter.

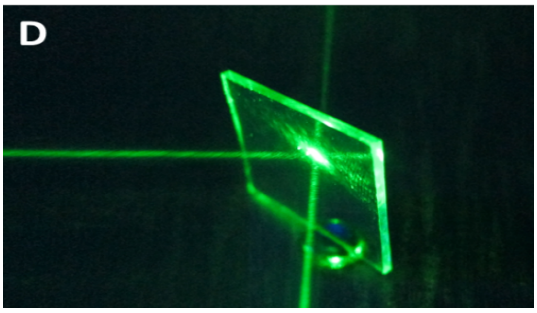

Fig.16: Plate beam splitter (or half-silvered mirrors).

6.3. ***Photodiode as detector***

A photodiode is a semiconductor P-N junction diode, it acts as a light sensor by converting incoming light energy into electrical energy.

6.3.1. Working mechanism :

A p-n junction diode always operates in reverse bias mode but, in the absence of external voltage it has a diode potential across the depletion region, and in a silicon based diode this potential is around 0.7V. Now when external potential difference is applied across it in reverse bias configuration, the depletion region expands until the depletion potential across the diode becomes equal to the applied external voltage.

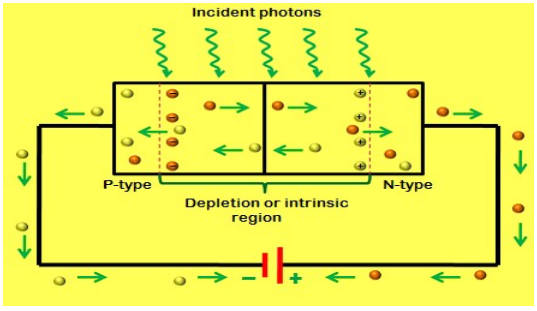

Fig.17: Schematic of a working Photo-diode .

Now when light is illuminated on the diode (specifically the depletion region), the photons hit the recombined electrons and knock them out, the knocked out electrons get pulled due to the potential and a current flow is observed which results in shrinking of the depletion region. The current flow can be measured across a load and this voltage is known as "*reverbiasing current*".

Now depending upon this property the photodiode generates the electrical current as a response to the bright fringes in Michelson interferometer, and no current is generated for dark

fringes.

The reverse-bias current in general is very small, so for better sensitivity we are using the following circuit with operational amplifier(Op-amp) to amplify the output reverse biasing current. Figure 17 shows the circuit diagram with included Op-amp.

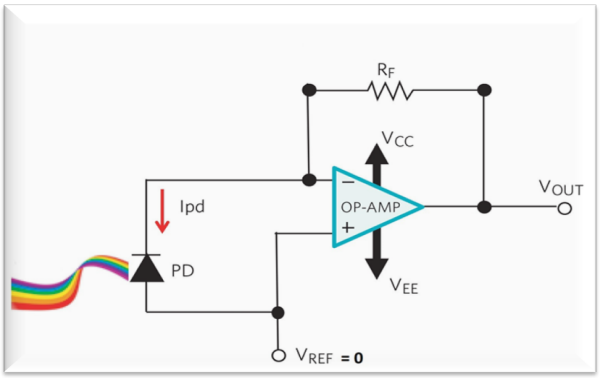

Fig. 18: Photodiode with external circuit.

6.3.2. **Smart table mechanism**

6.4. ***Active Damped Smart Optical Table***

SmartTable optical table tops feature two IQ active dampers which effectively address medium frequency resonances of optical tables by sensing the vibrations and driving shakers at the opposite phase of the vibrations to cancel them out. Broadband damping is provided by a 4.8 mm thick table skin, a constrained layer core that attenuates broadband vibration, a damped working surface that eliminates skin resonance, and a composite edge finish that eliminates sidewall resonance.

Fig. 19: SmartTable Optical table (@NISER).

6.4.1. **Smart table mechanism**

In the experiment we are using SmartTable as vibrations causes disturbance of focused light beam on the detector.

At the core of the SmartTable optical table tops is an advanced damping technology called Intelligent Q (IQ) Damping. It effectively addresses the medium frequency resonances of optical tables from 80 to 550 Hz by incorporating two pairs of sensors and actuators in the optical table top design. An external controller is used to coordinate the signal processing, enabling a fast and accurate damping response. Each sensor-actuator pair is controlled by a separate control channel. The sensor senses the vibrations and the actuator outputs a signal to compensate for the vibrations (Figure 19).

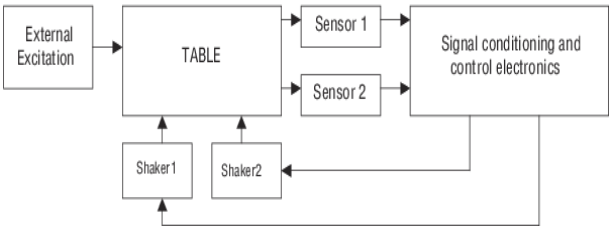

Fig. 20: Schematic of Intelligent Q (IQ) Active Damping Technology.

The pre-amplifiers and band-pass filters condition the sensor output signal before feeding it to the digital controller. The digital controller implements recursive filters that compensate for the dynamic response of the shaker and correct the phase to bring the phase difference between the displacement and force close to $(-\pi/2)$ in the desired frequency range.

6.5. ***Solenoid***

In the experiment a long solenoid is used to generate magnetic field. The magnetic field generated due to a solenoid of infinite length is given as:

$$H = \mu \frac{NI}{l} \tag{14}$$

where, **N** is the no.of turn in the coil, **I** is the current and **l** is the length of the coil.

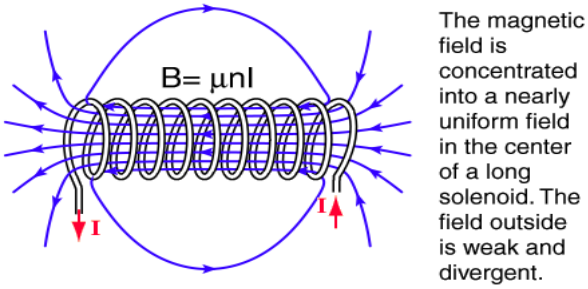

Fig. 21: Magnetic field generated in a solenoid.

Magnetic field generated due to a finite length solenoid is given as:

$$H = \frac{NI}{\sqrt{\left(4r^2 + l_S^2\right)}} \tag{15}$$

where, **N** is the no.of turn in the coil, **I** is the current andl_s is the length of the finite coil. This formula can be derived through Biot-Savart's law via considering one rotation as a single source.

6.6. ***LabVIEW for measurement***

LabVIEW is a system-design platform and development environment for a visual programming language from National Instruments. LabVIEW offers a graphical programming approach that helps visualize every aspect of application, including hardware configuration, measurement data, and debugging.

6.6.1. **Why LabVIEW?**

LabVIEW has new features that improve interoperability with Python and MATLAB, developing Real-Time and FPGA applications, and software engineering. Additionally, includes enhancements in block diagram wiring and front panel visualizations plus preventing automatic application execution.

7. Addressing the questions asked during the presentation

1. Why do fringes become closer to each other at larger radius?
Fringes are defined as the distance between two consecutive destructive interferences. From (9), we can cook up the condition for destructive interference as:

$$\delta x = \frac{2n+1}{2}\lambda = 2d\,\mathrm{Cos}\,(\theta_n)$$

If we have nth destruction at θ_n and n − 1 th destruction at θ_{n-1}, we have

$$x_{\text{fringe}} = \frac{2n+1}{2}\lambda - \frac{2(n-1)+1}{2}\lambda = 2d\,\mathrm{Cos}\,(\theta_n) - 2d\,\mathrm{Cos}\,(\theta_{n-1})$$
$$\Rightarrow x_{\text{fringe}} = 2d\,(\mathrm{Cos}\,(\theta_n) - \mathrm{Cos}\,(\theta_{n-1}))$$

For larger radius θ_n and θ_{n-1} tends closer to $\frac{\pi}{2}$. Hence, both the cosine terms tend to 0 and the fringes merge together at $r \to \infty$.

2. Why does iron have changing magnetostriction?

While the exact reason is still unclear, we feel it is due to the anisotropy of the Fe crystal. Iron has two forms of lattice structure stable at room temperature: BCC and FCC. The magneto stress generates easy axes based on the lattice symmetry existing in our material. If Fe has a composition of both these structures then it might lead to a slight positive magnetostriction at the start and behave like Ni at larger field strengths. Again, since we are unsure if our commercially available iron has both the crystal arrangements, we are not sure if our explanation holds true here...

3. Do we have a theoretically calculated formula for stress generated by **H** for various ferromagnetic materials?

It is extremely difficult to obtain a theoretical formula to describe the effect of magnetostriction of a material. This process is sensitive to our sample's lattice arrangement, the exchange interaction, and many other lattice level defects that affect the potential landscape of the crystal, and hence the overall crystal energy. While it is possible to theoretically explain why this phenomenon exists, it is hard to incorporate all these factors and hold them inside a single formula (other than (5)).

4. Why does Op-amp operate in negative feedback?

We operate our op-amp in negative feedback mode as we want to stabilise the output voltage to a constant amplification value. If it is operated in positive feedback mode, then the slightest voltage change in the input terminals lead to a constant addition of it at every loop and quickly reach the maximum voltage, irrespective of the amount of current flowing. But if we operate it in negative feedback, any slight decrease in voltage produces an opposite positive voltage in one iteration and brings it back to an equilibrium around V_{out}. Hence that is the mode which is used in our Op-Amp.

8. Conclusion and future work

This report discusses the detailed theory of magnetostriction in the lattice due to existing symmetries and anisotropies that drive the system to realign its domains and create magnetic stress with specific symmetric components depending on the lattice arrangement. On considering only the longitudinal magnetostriction and neglecting rotational stress, we arrived at (eqn.5) that relates strain due to the generated magneto stress as a function of applied magnetic field H. To measure the expected strain we take aid of Michelson interferometer whose theory has also been discussed and as a conclusion from various simulations, we also discussed the properties of the fringes formed and precautions to prevent obtaining non-circular fringes in the process. We measure the length change in our material by counting the no.of fringes at the center with the help of a photodiode. We also discussed the details of the main apparatus used and why we prefer those components in our experiment. We also answered the questions asked during our presentation. In future, we wish to explore, on our hands-on experiments the effect of heating by changing the rate at which current is changed in the solenoid. We would also investigate the effect of premagnetisation in our sample, and try to optimise the Photodiode detection, if deemed necessary. If time permits, we would also try to discuss with professors and see if torsional strain will be possible to measure in our ferromagnetic samples.

9. References

1. Alex Hubert, Rudolf Schafer. Magnetic Domains: The analysis of Magnetic Microstructures. ISBN 978-3-540-64108-7 Springer Berlin Heidelberg New York(2009)
2. NISER Laboratory manuals.